Characterization and Reactivity of Molybdenum Oxide Catalysts Supported on Niobia†

Komandur V. R. Chary,* Thallada Bhaskar, Gurram Kishan, and Kondakindi Rajender Reddy

Catalysis Division, Indian Institute of Chemical Technology, Hyderabad 500 007, India

Received: September 11, 2000; In Final Form: December 28, 2000

A series of MoO_3/Nb_2O_5 catalysts with Mo loadings varying from 2.5 to 15 wt % were prepared and characterized by X-ray diffraction (XRD), temperature-programmed reduction (TPR), temperature-programmed desorption (TPD) of ammonia, electron spin resonance (ESR), oxygen chemisorption, and pore size distribution measurements. X-ray diffraction patterns indicate the presence of a crystalline molybdenum phase at higher Mo loadings on niobia. Dispersion of molybdenum was determined by the oxygen chemisorption at 623 K by a static method on the samples prereduced at the same temperature. At low Mo loadings, i.e., <10.0%, molybdenum oxide is found to be present in a highly dispersed state. Pore size distribution studies indicate a decrease in average pore diameter and pore volume with increased Mo loading. ESR results suggest the presence of Mo^{5+} in the reduced catalysts. TPR results suggest that the reducibility of MoO_3 increases with increased Mo loading. The reduction peaks due to niobia in TPR appeared at high temperatures (>1173 K) and their intensity decreases with Mo loading. TPD of ammonia results suggest that acidity of the catalysts was found to increase with increased molybdenum loading. The catalytic properties were evaluated for the vapor-phase ammoxidation of 3-picoline to nicotinonitrile and related to oxygen chemisorption sites.

Introduction

Catalysts containing molybdenum oxide/sulfide as an active component have been extensively employed in the recent past for the partial oxidation of hydrocarbons and alcohols and also extensively used in hydroprocessing reactions for petroleum industry.[1−15] The development in petroleum refining technology in the last three decades has raised hydroprocessing reactions to a high level of economic importance. The catalytic properties of the active molybdenum oxide phase can be greatly influenced by the nature of the supported oxide and the dispersion of active component. The most commonly used supports are alumina,[16−18] silica,[7,9−10,19−21,38] titania,[11,15,22−24,36] and zirconia.[25−27] In recent years niobium-based materials have been employed as catalysts in numerous catalytic applications.[28−34] Niobia can be used as support, as promoter, and as a unique solid acid. Smits[33] emphasized the advantages of niobia as a catalyst support for vanadia. These include the following: (i) Niobium is in the same group of the periodic table as vanadium or molybdenum and is expected to have similar properties. (ii) Niobium is much more difficult to reduce than vanadium or molybdenum (easy reduction often causes low selectivity in selective oxidation reactions). (iii) The addition of niobium oxide to a mixture of molybdenum and vanadium oxides improves the activity and selectivity for oxidation, ammoxidation, and oxidative dehydrogenation reactions.[33,34] Huuhtanen et al.[31] reported a comparison of different supports, and niobia appears to be promising as for as selectivity in toluene oxidation was concerned. Matsuura et al.[14] reported that the catalytic activity during the ammoxidation of isobutane to methacrylonitrile was improved when the Bi−Mo-based composites were supported on Nb_2O_5 rather than γ-Al_2O_3 or SiO_2.

The study of determining the dispersion of active phase in supported metal oxide systems is an interesting topic of research in recent years for understanding the role of the active phase on catalytic activity/selectivity during the oxidation reactions. A fundamental understanding of the structure−activity relationships observed in heterogeneous catalytic oxidation is of basic importance for the development of new catalytic materials and for improving the performance of existing catalysts.[35] To this end, methods such as oxygen chemisorption have been studied extensively in recent years to find active phase dispersion in supported metal oxide systems.

In the present investigation we report the characterization of MoO_3/Nb_2O_5 catalysts by powder X-ray diffraction (XRD), oxygen chemisorption and pore size distribution measurements (PSD), electron spin resonance (ESR), temperature-programmed reduction (TPR), and temperature-programmed desorption (TPD). The catalytic properties have been evaluated for the ammoxidation of 3-picoline to nicotinonitrile. We also report the relation between dispersion of molybdenum oxide and catalytic properties of the catalysts during vapor phase ammoxidation of 3-picoline to nicotinonitrile. The purpose of this work is to estimate the dispersion of molybdenum oxide supported on niobia as a function of molybdenum loading and to identify the changes in structure of the molybdena phase with increased active phase loading and also to understand the relation between activity/selectivity and oxygen chemisorption sites.

Experimental Section

Catalyst Preparation. A series of MoO_3 catalysts with Mo loadings ranging from 2.5 to 15 wt % supported on Nb_2O_5 (surface area 55 $m^2\ g^{-1}$) were prepared by incipient wetting of the support with aqueous ammonium heptamolybdate (Fluka AG, Switzerland) solution at pH 8. The catalysts were subsequently dried at 383 K for 16 h and calcined in air at 773 K for 6 h. The niobium pentoxide hydrate (niobia HY-340 AD/1227,

† IICT Communication Number 4586.

* To whom correspondence should be addressed: e-mail kvrchary@iict.ap.nic.in.

10.1021/jp003201y CCC: $20.00
Published on Web 04/19/2001

CBMM, Brazil) was calcined in air at 773 K for 4 h before impregnation with ammonium heptamolybdate.

X-ray Diffraction and Electron Spin Resonance. ESR spectra were recorded at ambient temperature on a Bruker ER-200D-SRC X-band spectrometer with 100 kHz modulation. The reduced catalysts for the ESR study were prepared in quartz tubes (25 cm long, 4 mm diameter). The samples were prereduced at 623 K for 2 h in a continuous flow (40 mL/min) of purified hydrogen. The setup was subsequently evacuated for 1 h at 10^{-6} Torr. The catalyst thus prepared was transferred to the ESR tube and sealed off under vacuum. X-ray diffraction patterns were recorded on Siemens D-5000 X-ray diffractometer with graphite-filtered Cu Kα radiation.

Oxygen Chemisorption. Oxygen chemisorption was measured by a static method with an all-Pyrex glass system capable of attaining a vacuum of 10^{-6} Torr. The details of the experimental set up are given elsewhere.[36] Before adsorption measurements, the samples were prereduced in a flow of hydrogen (40 mL/min) at 623 K for 2 h and evacuated at the same temperature for 1 h. Oxygen chemisorption uptakes were determined as the difference of two successive adsorption isotherms measured at 623 K. The surface areas of the catalysts were determined by the BET method with nitrogen physisorption at 77 K, taking 0.162 nm^2 as its cross-sectional area. Pore size distribution (PSD) measurements were performed on Auto Pore III (Micromeritics) by the mercury penetration method.

Temperature-Programmed Reduction. TPR studies were conducted on AutoChem 2910 (Micromertitics) instrument. The unit has a programmable furnace with a maximum operating temperature of 1373 K. The instrument was interfaced with a computer that performs tasks such as programmed heating and cooling cycles, continuous data recording, gas valve switching, data storage, and analysis.

In a typical TPR experiment about 250 mg of MoO_3/Nb_2O_5 sample dried at 383 K for 16 h was taken in a U-shaped quartz sample tube. The catalyst was packed on a quartz wool plug in one arm of the sample tube. The temperature was monitored with the aid of thermocouples located near the sample from outside and on the top of the sample. The gas flows were monitored by highly sensitive mass-flow controllers. Before TPR studies the catalyst samples were pretreated by passage of ultra-high-purity helium (50 mL/min) at 673 K for 2 h. After pretreatment the sample was cooled to room temperature. The reducing gas consists of 5% hydrogen and balance argon (50 mL/min), which was purified by passage through oxy-trap and molecular sieves. The water produced during reduction was condensed in a cold trap kept in a liquid nitrogen and 2-propanol slurry. The hydrogen concentration in the effluent stream was monitored with the thermal conductivity detector, and the areas under the peaks were integrated by use of GRAMS/32 software to determine hydrogen consumption. T_{max} calibration of the TCD was performed by stoichiometric reduction of a known amount of high-purity Ag_2O to metallic silver, a method that was found to be more reliable and reproducible than sending the known volumes of hydrogen pulses through the reactor.

Temperature-Programmed Desorption. In a typical experiment for TPD studies, about 200 mg of oven-dried sample (dried at 383 K for 16 h) was taken in a U-shaped quartz cell. The catalyst sample was packed in one arm of the sample tube on a quartz wool bed. The temperature was monitored with the aid of thermocouples located near the sample from outside and one on the top of the sample. The gas flows were monitored by highly sensitive mass-flow controllers. Prior to TPD studies, the catalyst sample was pretreated by passage of high-purity helium (50 mL/min) at 473 K for 2 h. After pretreatment, the sample was saturated by passage of highly pure anhydrous ammonia (75 mL/min) at 353 K and subsequently flushed at 378 K for 2 h to remove the physisorbed ammonia. TPD analysis was carried out from ambient temperature to 1073 K at a heating rate of 10 K/min. The ammonia concentration in the effluent stream was monitored with the thermal conductivity detector and the areas under the peaks were integrated by use of GRAMS/32 software to determine the amount of desorbed ammonia during TPD. TCD calibration was performed by an automated experiment by passing known volumes of ammonia.

Ammoxidation of 3-Picoline. A downflow fixed-bed reactor operating at atmospheric pressure and made of Pyrex glass was used to test the catalysts during the ammoxidation of 3-picoline to nicotinonitrile. About 2 g of the catalyst diluted with an equal amount of quartz grains was charged into the reactor and was supported on a glass wool bed. Prior to introduction of the reactant 3-picoline with a syringe pump (B-Braun perfusor), the catalyst was reduced at 723 K for 2 h in purified hydrogen flow (40 mL/min). After the prereduction the reactor was fed with 3-picoline, ammonia, and air, keeping the mole ratio of 3-picoline:H_2O:NH_3:air at 1:13:11:44. The reaction was carried out at various temperatures ranging from 573 to 723 K. The liquid products, mainly nicotinonitrile, were analyzed by the HP 6890 gas chromatograph equipped with an FID using OV-17 column.

Results and Discussion

The X-ray diffraction patterns of calcined MoO_3/Nb_2O_5 catalysts are presented in Figure 1. In all the samples XRD peaks due to low-temperature niobia were observed at $d = 3.95$, 3.14, 2.45, 1.97, and 1.66 Å. At higher Mo loadings (above 7.5 wt % Mo, Figure 1d), XRD peaks due to the crystalline MoO_3 phase are noticed at $d = 3.26$ and 3.81 Å, in addition to the characteristic peaks of niobia. The intensity of these peaks increases with MoO_3 loading. However, at low Mo loading the absence of crystalline MoO_3 peaks cannot be ruled out as they might be less than 40 Å in size, which is beyond the detection capacity of the XRD technique. XRD results also suggest that no mixed oxide is formed between MoO_3 and Nb_2O_5. The two low-temperature forms of Nb_2O_5, i.e., TT and T, have long thought to be the same,[37] because (i) they have similar X-ray diffraction patterns and (ii) the TT phase does not always appear with pure components as starting materials. According to Ko and Weissman,[37] TT phase may be a crystalline form of T, stabilized by impurities. Ko and Weissman[37] also reported that, at low calcination temperature (773 K), the samples are found to be X-ray amorphous. However, the samples calcined between 773 and 873 K show the TT phase of Nb_2O_5, and the samples calcined between 873 and 973 K favor the formation of the T phase of Nb_2O_5. At 1073 K calcination, the M phase of Nb_2O_5 is observed, and at 1273 K and above, the H phase of Nb_2O_5 is observed. In the present study, the samples were calcined at 773 K and our XRD results (Figure 1) also suggest the formation of the TT phase of Nb_2O_5, which is in good agreement with the work of Ko and Weissman.[37] However, although the d spacing of TT and T phases of Nb_2O_5 is similar, the intensities of d spacing are different. At $d = 3.94$ Å the intensities were found to be 100 and 84 for TT and T phases, respectively. However, at $d = 3.13$ Å the intensities were found to be 90 and 100 for TT and T phases. The intensities of d spacings in the present XRD patterns (Figure 1) suggest that only the TT phase of Nb_2O_5 is observed. XRD patterns of pure MoO_3 and pure Nb_2O_5 are shown in Figure 2. Pure Nb_2O_5 shows intense

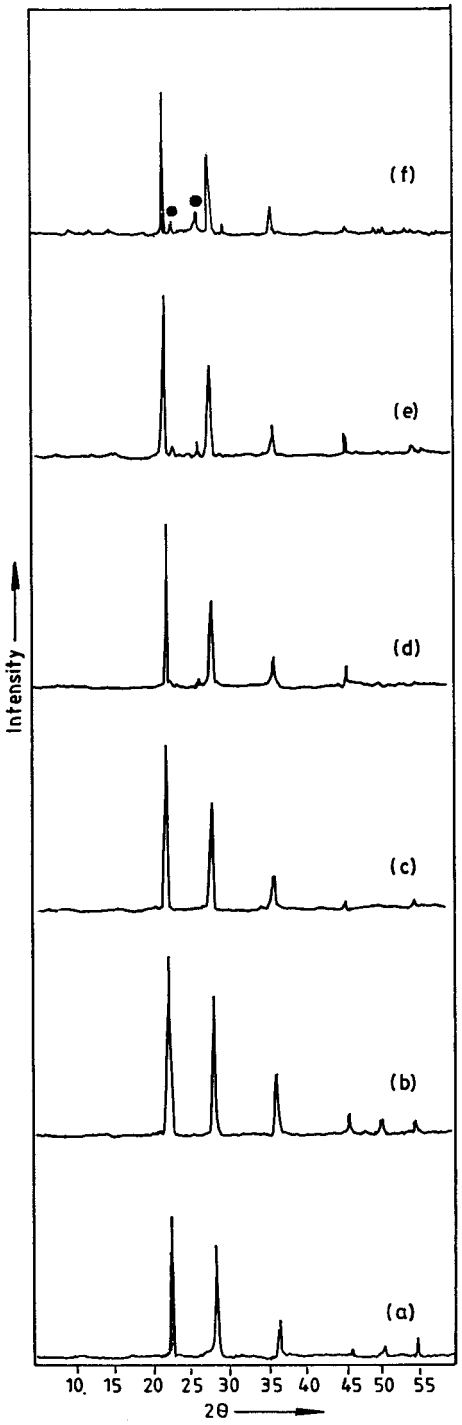

Figure 1. X-ray diffractograms of MoO_3/Nb_2O_5 catalysts: (a) 2.5% Mo/Nb_2O_5; (b) 5.0% Mo/Nb_2O_5; (c) 7.5% Mo/Nb_2O_5; (d) 10.0% Mo/Nb_2O_5; (e) 12.5% Mo/Nb_2O_5; (f) 15.0% Mo/Nb_2O_5. Solid circles indicate peaks due to MoO_3.

diffraction peaks at $d = 3.95$ and 3.14 Å, due to the T phase of Nb_2O_5. Similarly pure MoO_3 show intense peaks at $d = 3.26$, 3.81, and 3.46 Å. The present XRD results are in good agreement with our earlier studies on Mo/TiO_2[67] and Mo/ZrO_2[68] catalysts, wherein crystalline MoO_3 appeared above monolayer coverage. Desikan et al.[38,45] also reported the appearance of crystalline MoO_3 at higher Mo loadings in MoO_3/SiO_2,[38] $MoO_3/TiO2$,[45] and MoO_3/Al_2O_3[45] catalysts.

The specific surface areas determined by nitrogen physisorption of all the catalysts are presented in Table 1. The specific surface area decreases as a function of molybdena content on

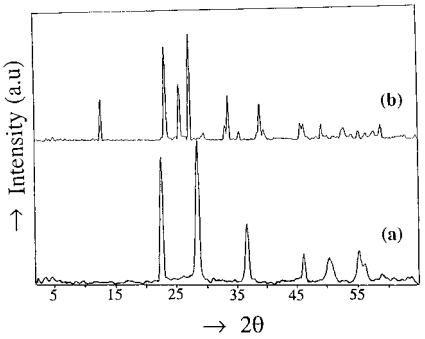

Figure 2. X-ray diffractograms of pure MoO_3 and pure Nb_2O_5 samples: (a) Nb_2O_5; (b) MoO_3.

TABLE 1: Results of Oxygen Uptake, Dispersion, Oxygen Atom Site Density, and Surface Area of Various MoO_3/Nb_2O_5 Catalysts

catalyst composition (wt % Mo)	surface area[a] ($m^2\ g^{-1}$)	oxygen uptake[b] (μmol g^{-1})	oxygen atom site density ($\times 10^{18}\ m^{-2}$)	dispersion[c] (O/Mo)
2.5	50	127.9	2.69	0.98
5.0	44	248.6	6.23	0.93
7.5	40	369.2	11.32	0.94
10.0	38	472.1	15.64	0.90
12.5	29	545.4	21.73	0.83
15.0	27	604.5	30.65	0.77

[a] BET surface area determined after oxygen chemisorption. [b] $T_{(reduction)} = T_{(adsorption)} = 623$ K. [c] Dispersion = fraction of molybdenum atoms at the surface assuming $O_{ads}/Mo_{surf} = 1$.

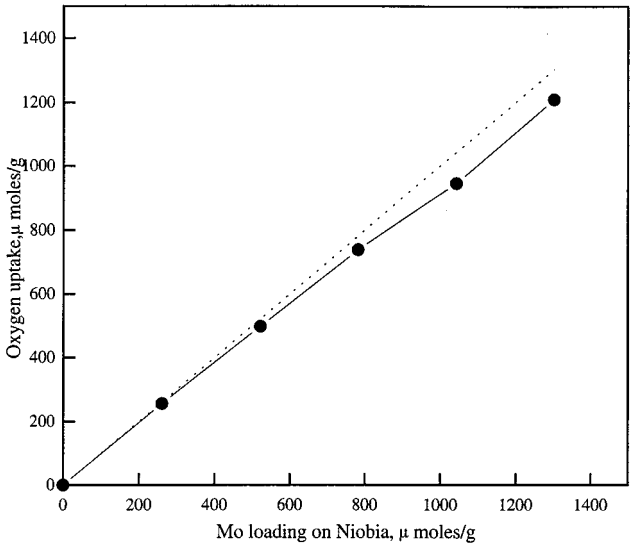

Figure 3. Oxygen uptake plotted as a function of Mo loading on Niobia. ($T_{adsorption} = T_{reduction} = 623$ K).

niobia and it might be due to blocking of the pores of the support by crystallites of niobium oxide and also molybdena as evidenced by XRD and PSD. The oxygen chemisorption uptake results of various catalysts are also presented in Table 1 and the other information, such as oxygen atom site density, dispersion, etc., derived from it are also given in Table 1. The oxygen atom site density, defined as the number of oxygen atoms chemisorbed per unit area of the reduced MoO_3 surface, was found to increase with increased Mo loading.

Figure 3 shows the oxygen uptake measured at 623 K for various MoO_3/Nb_2O_5 catalysts plotted as a function of Mo content on niobia. The oxygen chemisorption uptakes are found to increase with increased molybdena content. The dispersion of molybdena was found to decrease steadily with increased

molybdena content. In Figure 3, the dashed line corresponds to a stoichiometry of one oxygen atom per molybdenum atom. Pure Nb_2O_5 was also reduced under identical conditions and its oxygen uptake was corrected for the supported catalysts. Dispersion of molybdena is defined as the fraction of total O atoms to total Mo atoms in the sample. The dispersion was found to be 98% for 2.5 wt % Mo/Nb_2O_5 and 77% for 15 wt % Mo/Nb_2O_5. These findings are in excellent agreement with the oxygen chemisorption results of Oyama and co-workers[38] on molybdena supported on silica and also with our earlier studies on MoO_3/TiO_2.[36] The decrease of Mo dispersion at higher loadings might be due to formation of microcrystalline MoO_3 in addition to niobia as evidenced from XRD results.

The reduction behavior of supported molybdena catalysts prior to oxygen chemisorption is an interesting topic. Many authors have reported the reduction of molybdena at 773 K followed by oxygen chemisorption at 195 or 77 K for determining dispersion of molybdena.[11,39−43] These conditions were evaluated by Rodrigo et al.,[44] who concluded that oxygen chemisorption under these conditions does not provide a quantitative determination of Mo dispersion because a fraction of the reduced Mo is in the bulk. It has been shown recently that oxygen chemisorption sites are easily generated under very mild reduction conditions.[38,45,46]

We have calculated the theoretical monolayer capacity of MoO_3 supported on Nb_2O_5 based on the method described by Van Hengstum et al.[47] taking 0.16 wt % MoO_3/m^2 of surface. Accordingly, the theoretical monolayer capacity of MoO_3 supported on niobia employed in the present study having a surface area of 55 $m^2\ g^{-1}$ corresponds to 8.8% MoO_3 or 5.86% Mo. However, XRD results from the present work show the presence of MoO_3 crystallites from 10.0 wt % Mo (Figure 1d), which indicates the formation of monolayer and is in good agreement with the theoretical monolayer based on the structure of MoO_3. In the present study the leveling off of oxygen chemisorption beyond the monolayer composition (above 6% Mo loading) might be due to the presence of the larger crystallites of MoO_3 as evidenced from the X-ray diffraction results (Figure 1d−f). These larger crystallites of molybdenum oxide are preventing reduction of the catalyst with hydrogen gas; therefore, no appreciable change in oxygen uptake is observed for the catalysts beyond the monolayer composition.

Figure 4 represents incremental intrusion volume vs pore diameter of various MoO_3/Nb_2O_5 samples. All the samples show bimodal distribution with the majority of pores present in the large pore diameter range (>1000 Å). However, the small amount of volume is also concentrated in the median pore region. As the molybdena loading is increased, the population of median pores is also found to increase in the catalysts. It has been observed that the average pore diameter increases marginally with MoO_3 loading. This change might be due to blockage of pores, which can be noticed from the decrease in the intensity of pores. Similarly, the total pore area also decreases with addition of MoO_3. The details of total pore area, total intrusion volume, and average pore diameter of MoO_3/Nb_2O_5 catalysts are reported in Table 2. The reactants and products (3-picoline and nicotinonitrile) can easily pass through these median pores. The increase in the median pore population and increase in 3-picoline ammoxidation conversion with molybdena loading can be observed from Figures 3 and 9, respectively. This clearly indicates that the median pores play a vital role during the reaction.

The ESR results of the hydrogen-reduced catalysts further support the findings of oxygen chemisorption. The spectra of reduced catalysts recorded at 300 K are represented in Figure 5. In all the catalysts an axially symmetric spectrum appears at the center of the pattern with $g_{II} = 1.917$. The intensity of the anisotropic spectrum increased with Mo loading. The spectral features of hydrogen-reduced samples suggest the presence of Mo^{5+} and are in good agreement with earlier works.[48]

The TPR profile of unsupported MoO_3 is presented in Figure 6. The TPR profile of pure MoO_3 shows two major peaks at 1040 and 1270 K and one minor reduction peak at 1070 K. For TPR analysis of unsupported MoO_3, the reduction conditions

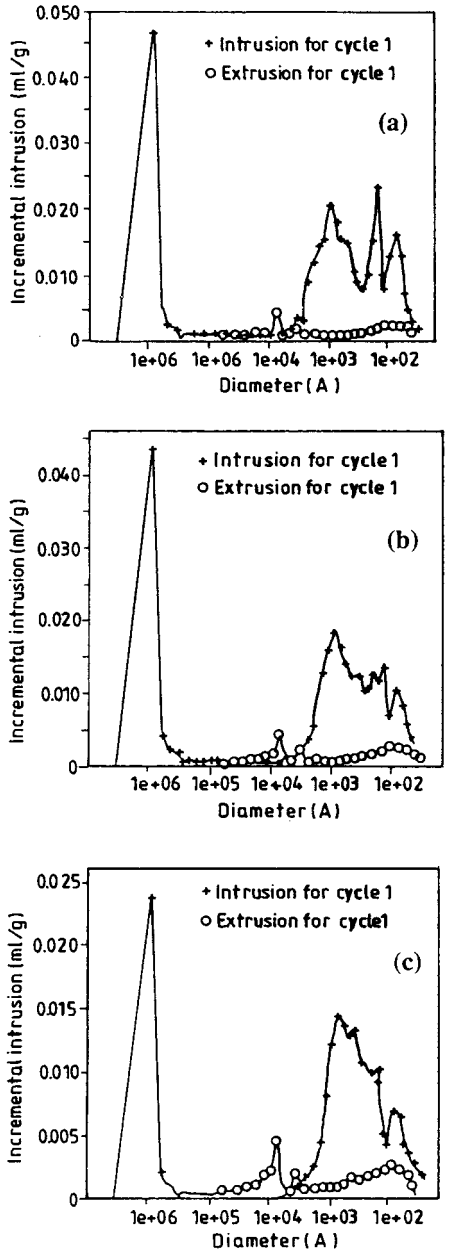

Figure 4. Pore size distribution (PSD) studies of MoO_3/Nb_2O_5 catalysts: (a) 2.5% Mo/Nb_2O_5; (b) 7.5% Mo/Nb_2O_5; (c) 12.5% Mo/Nb_2O_5.

TABLE 2: Results of Pore Size Distribution Analysis for MoO_3/Nb_2O_5 Catalysts

wt % Mo on Nb_2O_5	total intrusion volume (mL/g)	total pore area (m^2/g)	average pore diameter (Å)
2.5	0.3605	65.298	221
7.5	0.2971	46.664	255
12.5	0.2114	39.962	272

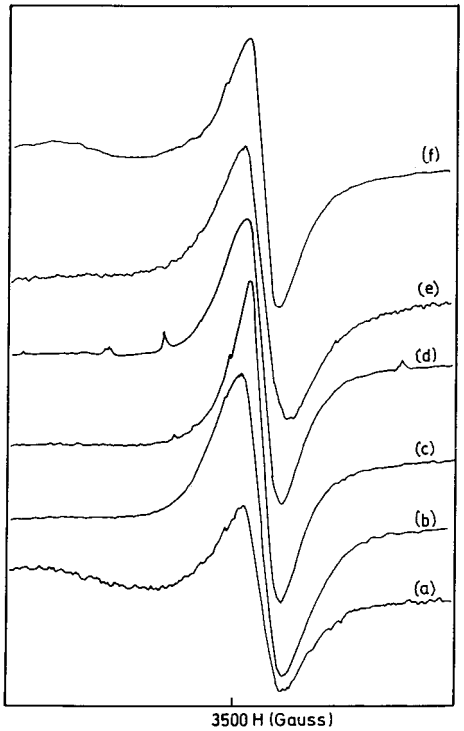

Figure 5. ESR spectra of hydrogen-reduced MoO_3/Nb_2O_5 catalysts: (a) 2.5% Mo/Nb_2O_5; (b) 5.0% Mo/Nb_2O_5; (c) 7.5% Mo/Nb_2O_5; (d) 10.0% Mo/Nb_2O_5; (e) 12.5% Mo/Nb_2O_5; (f) 15.0% Mo/Nb_2O_5.

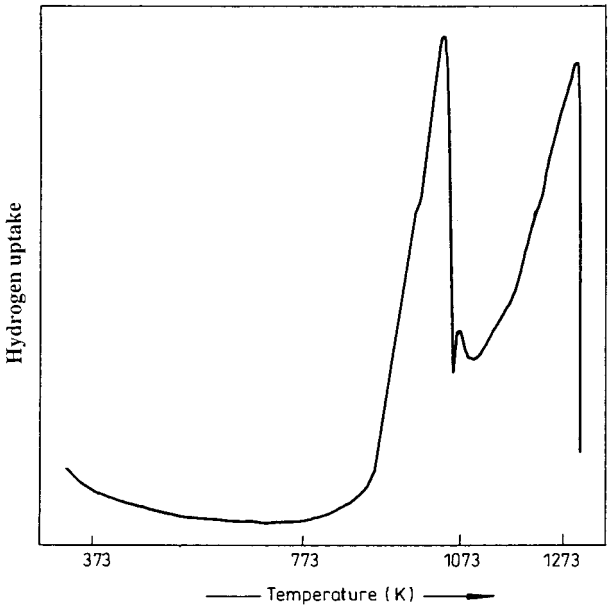

Figure 6. Temperature-programmed reduction (TPR) profile of unsupported MoO_3.

applied were similar to those for MoO_3/Nb_2O_5 catalysts. According to Thomas et al.[49] and Arnoldy et al.,[50] the reduction of molybdena essentially can take place in two steps. The reducibility of MoO_3 is represented by the following steps:

$$MoO_3 \rightarrow MoO_2 \quad (1)$$

The sharp peak at 1040 K corresponds to reduction of MoO_3

$$MoO_2 \rightarrow Mo \quad (2)$$

(first step) and the peak at 1270 K is associated with the reduction of MoO_2 (second step). A minor peak at the edge of

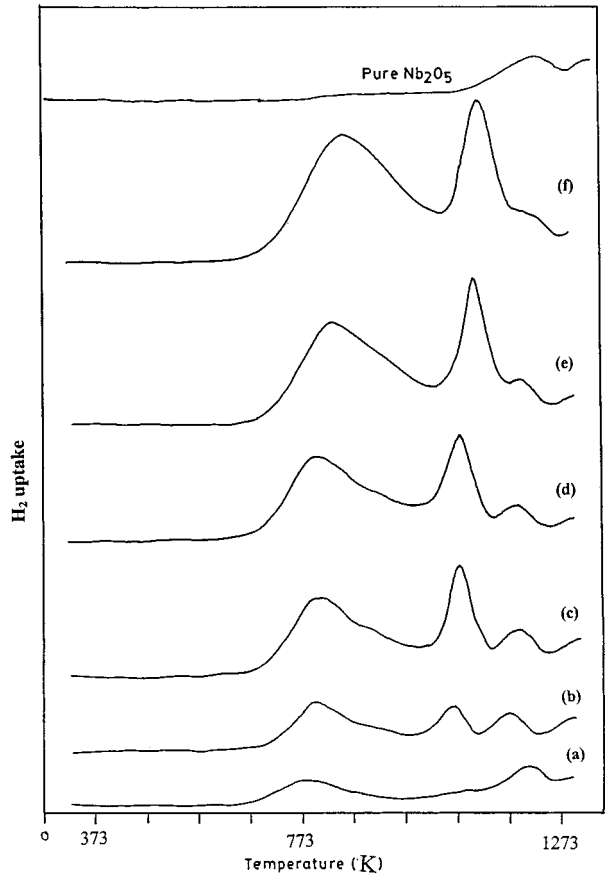

Figure 7. Temperature-programmed reduction (TPR) profiles of MoO_3/Nb_2O_5 catalysts: (a) 2.5% Mo/Nb_2O_5; (b) 5.0% Mo/Nb_2O_5; (c) 7.5% Mo/Nb_2O_5; (d) 10.0% Mo/Nb_2O_5; (e) 12.5% Mo/Nb_2O_5; (f) 15.0% Mo/Nb_2O_5.

the first major peak is observed at 1070 K, which corresponds to Mo_4O_{11} formed by reduction of MoO_3. Thomas et al.[49] also noticed the following peak, which was confirmed by in situ X-ray diffraction:

$$MoO_3 \rightarrow Mo_4O_{11} \quad (3)$$

Temperature-programmed reduction profiles of the niobia-supported molybdenum oxide catalysts are shown in Figure 7. TPR profiles of niobia-supported molybdenum oxide catalysts indicates that molybdena is reducing in two stages. The first peak T_{max} value increases with increased molybdena loading from 783 to 858 K, and also the area under the reduction peak increases with increased molybdenum loading. The T_{max} value for the second peak also increases with increased loading from 1063 to 1113 K, and the area under the reduction peak increases with increased molybdena loading. It is well-known that niobium oxide is partially reducible when exposed to hydrogen at high temperatures, and the reduction is accelerated by the presence of supported zerovalent metals on its surface. For this reason, metals supported on niobium oxide are known to exhibit strong metal−support interaction (SMSI) when reduced with hydrogen at high temperatures.[51−53] The reduction of Nb_2O_5 is partial and occurs around 1273 K. However, the reducibility of Nb_2O_5 becomes easier when it is associated with MoO_3, and this can be seen from Figure 7. On the other hand, the T_{max} for MoO_3 reduction in two stages is found to increase with MoO_3 loading on Nb_2O_5 surface. Compared to the bulk MoO_3 species, the reduction of MoO_3 species on Nb_2O_5 becomes much easier. It clearly indicates that there might be an interaction between

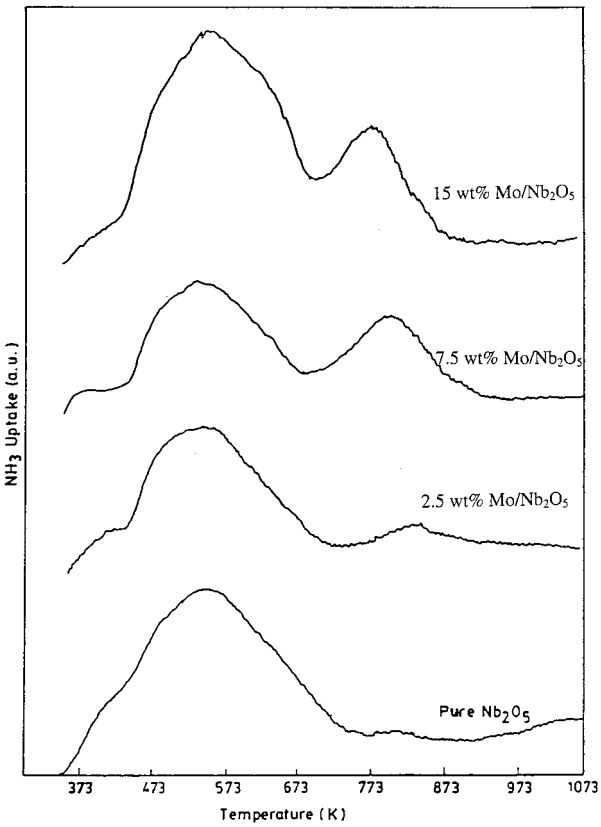

Figure 8. Ammonia temperature-programmed desorption (TPD) profiles of MoO_3/Nb_2O_5 catalysts: (a) Pure Nb_2O_5; (b) 2.5% Mo/Nb_2O_5; (c) 7.5% Mo/Nb_2O_5; (d) 15.0% Mo/Nb_2O_5.

TABLE 3: Results of Temperature-Programmed Desorption of Ammonia for MoO_3/Nb_2O_5

S no.	wt % Mo on Nb_2O_5	$T_{max}1$ (K)	NH_3 uptake (mL/g)	$T_{max}2$ (K)	NH_3 uptake (mL/g)
1	0.0	561	5.24		
2	2.5	553	4.07	826	0.42
3	7.5	537	3.38	805	1.70
4	15.0	554	6.37	785	1.60

MoO_3 and Nb_2O_5. However, no such compounds are observed from the powder X-ray diffraction patterns. Most probably the interacting species may be present in an amorphous phase. The TPR results thus suggest that the reducibility of molybdena increases with increased Mo loading in MoO_3/Nb_2O_5 catalysts.

Niobium supported on certain oxides has shown a remarkable promoter effect for decomposition of NO,[28] and niobium pentoxide treated at relatively low temperatures, T_t ($423 < T_t < 573$ K), is an effective catalyst for various reactions such as esterification, dehydration, and isomerization reactions.[54−57] The surface acidity of niobium materials has been studied by *n*-butylamine titration with Hammett indicators, by infrared spectroscopy of adsorbed pyridine,[54,58] and by volumetric and gravimetric analysis of adsorbed NH_3.[59] The surface of $Nb_2O_5 \cdot xH_2O$ contains both Lewis and Bronsted acid sites.[54,60] Thus it is interesting to study the acidity of the molybdenum oxide supported on niobia. In the present study, the acidity measurements have been carried out by the ammonia TPD method. Ammonia TPD profiles for pure Nb_2O_5 and some of the representative Mo/Nb_2O_5 catalysts are shown in Figure 8. The ammonia uptake by various Mo/Nb_2O_5 catalysts and the temperature positions are given in Table 3. The TPD profiles (Figure 8) suggest the strength of acid sites and their distribution in two temperature regions, i.e., 373−673 and 673−873 K. The acidic sites in the temperature region of 373−673 K are due to moderate acid sites, and those in the region of 673−873 K are due to strong acid sites. TPD results suggest that pure Nb_2O_5 is less acidic compared to Mo/Nb_2O_5 catalysts. The number of acid sites with moderate strength was found to increase with Mo loading on niobia. However, the NH_3 uptake due to strong acid sites (Table 3) was found to be almost equal for 7.5 and 15 wt % Mo/Nb_2O_5 catalysts. This behavior is in agreement with the catalytic activity beyond 7.5 wt % Mo loading, which did not change appreciably with increased Mo loading on niobia support. This clearly indicates that strong acid sites are responsible for picoline ammoxidation. The TPD results suggests that the strength of acid sites plays a crucial role in determining the catalytic activity during ammoxidation of 3-picoline, and the acidity of the catalysts is mainly due to the molybdena phase since ammonia uptake increases with increased molybdena loading. The relation obtained can be explained in terms of stable Bronsted-acid centers that chemisorb ammonia as NH_4^+ and are also of interest in the ammoxidation of 3-picoline.[61] Iizuka et al.[58] showed that the surface of $Nb_2O_5 \cdot nH_2O$ showed strong acidic character ($H_0 \leq -5.6$) even after heating in air at 373 K, but the strong acid sites disappeared at higher temperatures. The active sites on the catalysts heat-treated at moderate temperatures were ascribed mainly to Bronsted acid sites on the basis of the IR study of adsorbed pyridine, and it is known that the selectivity of products is very sensitive to the surface acidic and basic properties.[60]

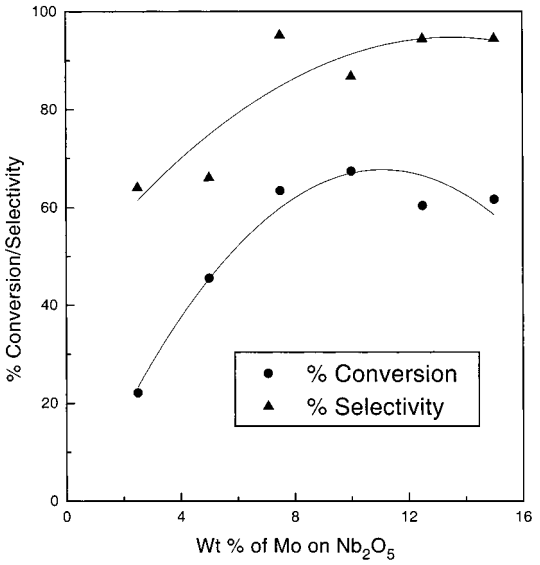

Figure 9. Ammoxidation of 3-picoline over MoO_3/Nb_2O_5 catalysts (reaction temperature 683 K).

Figure 9 shows the dependence of activity and selectivity on the molybdena loading during ammoxidation of 3-picoline to nicotinonitrile at 683 K. The catalytic experiments were repeated twice, and the values reported are the average of two sets of experiments. The conversion of 3-picoline is found to increase with Mo loading in the catalysts up to 7.5 wt % Mo loading. Beyond this loading the activity did not change appreciably. The selectivity toward nicotinonitrile formation is also found to increase with Mo loading. However, at high Mo loadings the selectivity remains unchanged. Pure Nb_2O_5 was also found to be active for the nicotinonitrile formation under the experimental conditions employed and corrected for the catalyst samples. The conversion of 3-picoline by pure Nb_2O_5 was found to be 3.14% and the product formed was only cyanopyridine. The contribution of pure Nb_2O_5 toward ammoxidation was subtracted from the conversion of MoO_3/Nb_2O_5 catalysts.

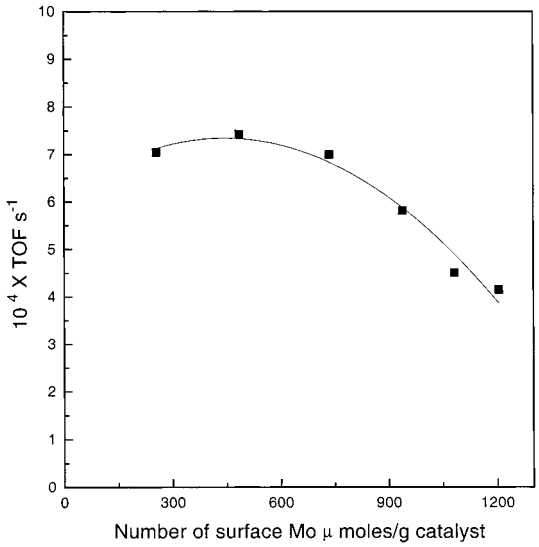

Figure 10. Relationship between the amount of surface Mo on Nb_2O_5 and the rate of 3-picoline conversion.

Several groups[62−64] studied the acid−base properties of supported vanadia catalysts in the ammoxidation of 3-picoline. It was found that high activity in the ammoxidation of 3-picoline corresponds to a relatively small amount of acidic sites. A catalyst selective in the formation of nicotinonitrile requires a high concentration of both acidic and basic sites. The conditions in the ammoxidation of 3-picoline are both reductive and oxidative; i.e., the hydrocarbons consume oxygen from the catalyst, which is then reoxidized. It can be expected that, under steady-state conditions, the catalyst will contain a certain amount of lower oxides formed by reduction of the originally charged catalyst.

To find the relation between the ammoxidation activity of 3-picoline and the dispersion of molybdena, a plot of TOF versus surface Mo content is shown in Figure 10, where TOF is defined as the number of picoline molecules converted per second per surface Mo. The TOF was found to be almost constant ($\approx 7 \times 10^{-4}$ s^{-1}) up to 7.5 wt % Mo and decreased at higher Mo loadings. Up to 7.5 wt % Mo loading, per-site activity (constant TOF) is constant with the increase in surface Mo sites. The decrease in TOF beyond 7.5 wt % Mo loading indicates the formation of bigger MoO_3 particles, but not enough to attain the bulk nature. The absence of direct correlation between TOF and amount of surface Mo may be due to the fact that, in addition to oxygen adsorption, ammonia adsorption may also be responsible for this reaction. A direct correlation was also reported earlier between oxygen uptake capacities of various vanadia[65,66] and molybdena[67] catalysts and nicotinonitrile product selectivity. As reported elsewhere in connection with molybdenum oxide catalysts supported on alumina[16] and on zirconia,[41] oxygen is chemisorbed at low temperatures selectively on coordinatively unsaturated sites (CUS), generated upon reduction, having a particular coordination environment. These sites are located on a highly dispersed molybdena phase, which is formed only at low molybdena loadings and remain as a "patchy monolayer" on the support surface. At higher molybdena loadings, a second phase is formed, in addition to the already existing monolayer, and this postmonolayer phase does not appreciably chemisorb oxygen (Figure 3). In the perspective of the above background, the correlation shown here indicates that the catalytic functionality of the dispersed molybdena phase supported on niobia that is responsible for the ammoxidation of 3-picoline to nicotinonitrile is located on a patchy monolayer phase, and this functionality can be titrated by the oxygen chemisorption method reported in this work.

Conclusions

The results of oxygen chemisorption suggest that molybdenum oxide is found to be highly dispersed on the niobia support. Pore size distribution studies indicated decreased average pore diameter and pore volume with increased Mo loading. TPR results demonstrated that the reducibility of MoO_3 increased with increased Mo loading in Mo/Nb_2O_5 catalysts. TPD of ammonia indicates the acidity falls into two regions, and acidity of the catalysts was found to increase with increased molybdena loading. The catalytic activity during 3-picoline ammoxidation can be related to dispersion of molybdena.

Acknowledgment. CBMM, Brazil, is gratefully acknowledged for providing the gift samples of Nb_2O_5. We thank Dr. K. V. Raghavan, Director, IICT, for encouragement. We are thankful to Dr. K. S. Rama Rao for helpful discussions. T.B. and G.K. thank the Council of Scientific and Industrial Research (CSIR), New Delhi, for the research associate (RA) positions, and K.R.R. thank CSIR, New Delhi, for a junior research fellowship (JRF).

References and Notes

(1) Massooth, F. E. *Adv. Catal.* **1978**, *27*, 265.
(2) Grange, P. *Catal. Rev. Sci. Eng.* **1980**, *21*, 135.
(3) Knozinger, H. In *Proceedings of the 9th International Congress on Catalysis*, Calgary, Canada, 1988; Phillips, M., Ternan, M., Eds; The Chemical Institute of Canada: Ottawa, Canada, 1989; Vol. 5, p 20.
(4) Reddy, B. M.; Chary, K. V. R.; Subrahmanyam, V. S.; Nag, N. K. *J. Chem. Soc. Faraday Trans. 1* **1985**, *81*, 1655.
(5) Ng, K. Y. S.; Gulari, E. *J. Catal.* **1985**, *95*, 33.
(6) Chung, J. S.; Miranda, R.; Bennett, C. O. *J. Catal.* **1988**, *144*, 898.
(7) Louis, C.; Tatibouet, J. M.; Che, M. *J. Catal.* **1988**, *109*, 354.
(8) Liu, Y. C.; Griffin, G. L.; Chan, S. S.; Wachs, I. E. *J. Catal.* **1985**, *94*, 108.
(9) Masuoka, Y.; Niwa, M.; Murakami, Y. *J. Phys. Chem.* **1990**, *94*, 1477.
(10) Zhang, W.; Desikan, A.; Oyama, S. T. *J. Phys. Chem.* **1995**, *99*, 14468.
(11) Chary, K. V. R.; Kumar, V. V.; Kanta Rao, P. *Langmuir* **1990**, *6*, 1549.
(12) Desikan, A. N.; Zhang, W.; Oyama, S. T. *J. Catal.* **1995**, *157*, 740.
(13) Miyata, H.; Mukai, T.; Ono, T.; Kubokawa, Y. *J. Chem. Soc., Faraday Trans. 1* **1988**, *84*, 4137.
(14) Matsuura, I.; Oda, H.; Hoshida, K. *Catal. Today* **1993**, *16*, 547.
(15) Quincy, B. R.; Houalla, M.; Proctor, A.; Hercules, D. M. *J. Phys. Chem.* **1990**, *94*, 1520.
(16) Nag, N. K. *J. Catal.* **1985**, *92*, 432.
(17) Wang, X.; Zhao, B.; Jiang, D.; Xie, Y. *Appl. Catal. A: Gen.* **1999**, *188*, 201.
(18) Vit, Z.; Zdrazil, M. *J. Catal.* **1997**, *171*, 305.
(19) Oyama, S. T.; Zhang, W. *J. Am. Chem. Soc.* **1996**, *118*, 7173.
(20) Arena, F.; Parmaliana, A. *J. Phys. Chem.* **1996**, *100*, 19994.
(21) Kikutani, Y. *J. Mol. Catal. A.: Chem.* **1999**, *142*, 265 and references therein.
(22) Miyata, H.; Mukai, T.; Ono, T.; Kubokawa, Y. *J. Chem. Soc., Faraday Trans.* **1988**, *84*, 4137.
(23) Machej, T.; Doumain, B.; Yasse, B.; Delmon, B. *J. Chem. Soc., Faraday Trans.* **1988**, *84*, 3905.
(24) Kim, D. S.; Segawa, K.; Soeya, T.; Wachs, I. E. *J. Catal.* **1992**, *136*, 539.
(25) Chen, K.; Xie, S.; Iglesia, E.; Bell, A. T. *J. Catal.* **2000**, *189*, 2.
(26) Calafat, A.; Avilan, L.; Aldana, J. *Appl. Catal. A: Gen.* **2000**, *201*, 215.
(27) Indovina, V. *Catal. Today* **1998**, *41*, 95.
(28) Tanabe, K. *Catal. Today* **1990**, *8*, 1.
(29) Tanabe, K.; Okazaki, S. *Appl. Catal. A: Gen.* **1995**, *133*, 191.
(30) Ross, J. R. H.; Smits, R. H. H.; Seshan, K. *Catal. Today* **1993**, *16*, 503.
(31) Huuhtanen, J.; Andersson, S. L. T. *Appl. Catal. A: Gen.* **1993**, *98*, 159.
(32) Smits, R. H. H.; Seshan, K.; Ross, J. R. H.; Kentgens, A. P. M. *J. Phys. Chem.* **1995**, *99*, 9169.

(33) Smits, R. H. H.; Seshan, K.; Ross, J. R. H.; Van den Oetelaar, L. C. A.; Helwegen, J. H. J. M.; Anantharaman, M. R.; Brongersma, H. H. *J. Catal.* **1995**, *157*, 584.

(34) Watling, T. C.; Deo, G.; Seshan, K.; Wachs, I. E.; Lercher, J. A. *Catal. Today* **1996**, *28*, 139.

(35) Peeters, I.; Denier van der Gon, A. W.; Reijme, M. A.; Kooyman, P. J.; de Jong, A. M.; van Grondelle, J.; Brongersma, H. H.; van Santen, R. A. *J. Catal.* **1998**, *173*, 28.

(36) Chary, K. V. R.; Bhaskar, T.; Kishan, G.; Vijaya Kumar, V. *J. Phys. Chem.* **1998**, *102*, 3936.

(37) Ko, E. I.; Weissman, J. G. *Catal. Today* **1990**, *8*, 27.

(38) Desikan, A. N.; Huang, L.; Oyama, S. T. *J. Phys. Chem.* **1991**, *95*, 10050.

(39) Parekh, B. S.; Weller, S. W. *J. Catal.* **1987**, *40*, 100.

(40) Lopez Agudo, A.; Gil-llambias, F. J.; Reyes, P.; Fierro, J. L. G. *Appl. Catal.* **1981**, *1*, 59.

(41) Reddy, B. M.; Chary, K. V. R.; Rao, B. R.; Sunandana, C. S.; Subrahmanyam, V. S.; Nag, N. K. *Polyhedron* **1996**, *5*, 191.

(42) Hall, W. K.; Millman, W. S. *J. Catal.* **1979**, *59*, 311.

(43) Hall, W. K.; Valyon, J. *J. Catal.* **1983**, *84*, 229.

(44) Rodrigo, L.; Marcinkowska, K.; Andot, A.; Roberge, P. C.; Kaliaguine, S.; Stencel, J. M.; Makowsky, L. E.; Deihl, J. R. *J. Phys. Chem.* **1986**, *90*, 2690.

(45) Desikan, A. N.; Huang, L.; Oyama, S. T. *J. Chem. Soc., Faraday. Trans.* **1992**, *88*, 3357.

(46) Gambaro, L. A.; Fierro, J. L. G. *React. Kinet. Catal. Lett.* **1981**, *18*, 495.

(47) Van Hengstum, A. J.; Van Ommen, J. G.; Bosch, H.; Gellings, P. J. *Appl. Catal.* **1983**, *5*, 207.

(48) Oliver, S. W.; Smith, T. D.; Pilbrow, J. R.; Pratt, K. C.; Christov, V. *J. Catal.* **1988**, *111*, 88.

(49) Thomas, R.; de Beer, V. H. J.; Moulijn, J. A. *Bull. Chim. Belg.* **1981**, *90*.

(50) Arnoldy, P.; de Jonge, J. C. M.; Mouljin, J. A. *J. Phys. Chem.* **1985**, *89*, 4517.

(51) Tauster, S. J.; Fung, S. C. *J. Catal.* **1978**, *55*, 29.

(52) Sankar, G.; Vasudevan, S.; Rao, C. N. R. *J. Phys. Chem.* **1988**, *92*, 1878.

(53) Weissman, J. G. *Catal. Today* **1996**, *28*, 159.

(54) Iizuka, T.; Ogasawara, K.; Tanabe, K. *Bull. Soc. Chem. Jpn.* **1983**, *56*, 2927.

(55) Chen, Z.; Iizuka, T.; Tanabe, K. *Chem. Lett.* **1984**, 1085.

(56) Ogasawara, K.; Iizuka, T.; Tanabe, K. *Chem. Lett.* **1984**, 645.

(57) Iizuka, T.; Fujie, S.; Ushikubo, T.; Chen, Z.; Tanabe, K. *Appl. Catal.* **1986**, *28*, 1.

(58) Okazaki, S.; Kurimata, M.; Iizuka, T.; Tanabe, K. *Bull. Chem. Soc. Jpn.* **1987**, *60*, 37.

(59) Kurosaki, A.; Okuyama, T.; Okazaki, S. *Bull. Chem. Soc. Jpn.* **1987**, *60*, 3541.

(60) Tanabe, K.; Misono, N.; Ono, Y.; Hattori, H. *Stud. Surf. Sci. Catal.* **1989**, *51*, 61.

(61) Andersson, A. *J. Catal.* **1982**, *76*, 144.

(62) Andersson, A.; Lundin, S. T. *J. Catal.* **1980**, *65*, 9.

(63) Vejux, A.; Courtine, J. *J. Solid State Chem.* **1978**, *23*, 93.

(64) Busca, G.; Cavani, F.; Trifiro, F. *J. Catal.* **1987**, *106*, 471.

(65) Chary, K. V. R.; Kishan, G.; Bhaskar, T.; Sivaraj, Ch. *J. Phys. Chem.* **1998**, *102*, 6792.

(66) Chary, K. V. R.; Kishan, G.; Bhaskar, T. *J. Chem Soc., Chem. Commun.* **1999**, 1339.

(67) Chary, K. V. R.; Bhaskar, T.; Kalyana Seela, K.; Srilakshmi, K.; Rajender Reddy, K. *Appl. Catal. A: Gen.* **2001** (in press).

(68) Bhaskar, T.; Rajender Reddy, K.; Praveen Kumar, C.; Murthy, M. R. V. S.; Chary, K. V. R. *Appl. Catal. A: Gen.* **2001**(in press).